Spatial Well-defined Metal-Corrole-Based Covalent Organic Polymers toward Remarkably Enhanced Multipurpose Electrocatalysis and High-Performance Zinc-Air Batteries

Yan-Fang Yao[a], Zhen-Yu Huang[a], Wan-Yue Xie[a], Si-Jing Huang[b*], Zheng-Yan Liu[a], Gang Yang[a], Jian-Shan Ye[a], Hai-Yang Liu[a]*, and Xin-Yan Xiao[a]*

[a] School of Chemistry and Chemical Engineering, Guangdong Provincial Key Laboratory of Fuel Cell Technology, South China University of Technology, Guangzhou 510641, China

[b] Analytical and Testing Center, South China University of Technology, Guangzhou 510641, China.

Corresponding authors:

E-mail addresses: czhsj@scut.edu.cn (S.J. Huang); chhyliu@scut.edu.cn (H.Y. Liu); cexyxiao@scut.edu.cn (X.Y. Xiao)

1. General Methods and Materials

All reagents were purchased from commercial suppliers and were used directly without further purification unless otherwise stated (pyrrole was freshly distilled before use). All solvents used in these experiments were reagent grades. Carbon black (CB, acetylene, 50% compressed, 99.9+%) was purchased from Alfa.

Zn-air battery fabrication

The anode was prepared using a polished Zn foil (0.25 mm). The air electrode was prepared using carbon cloth (CC) coated with Co-COP or Pt/Ir-based material. A hot press method was used to attach the CC (1.5 × 1.5 cm^2) onto the gas diffusion layer (GDL). for the cathode, a chemical ink was prepared using 2 mg Co-COP and 2 mg carbon black was dissolved in a mixture of 100 μL Nafion in 300 μL isopropanol. The solution was ultrasonicated for 1 h for thorough dispersion and deposited on the gas diffusion layer (GDL) (Toray Carbon 60, Alfa Aesar, 200 μm). Then, the acquired GDL

was dried under the infrared light. 6 M KOH and 0.2 M Zinc acetate were used as an aqueous electrolyte. The GDL geometric diameter was kept at 1 cm. The open circuit potential of Zn-air battery was measured directly when assembled with different catalysts. The performance was studied using galvanostatic charge-discharge and chronopotentiometry. For comparison, GDL was prepared using 2 mg Pt/C and IrO_2 by following a similar procedure as our polymer.

2. Synthesis procedures

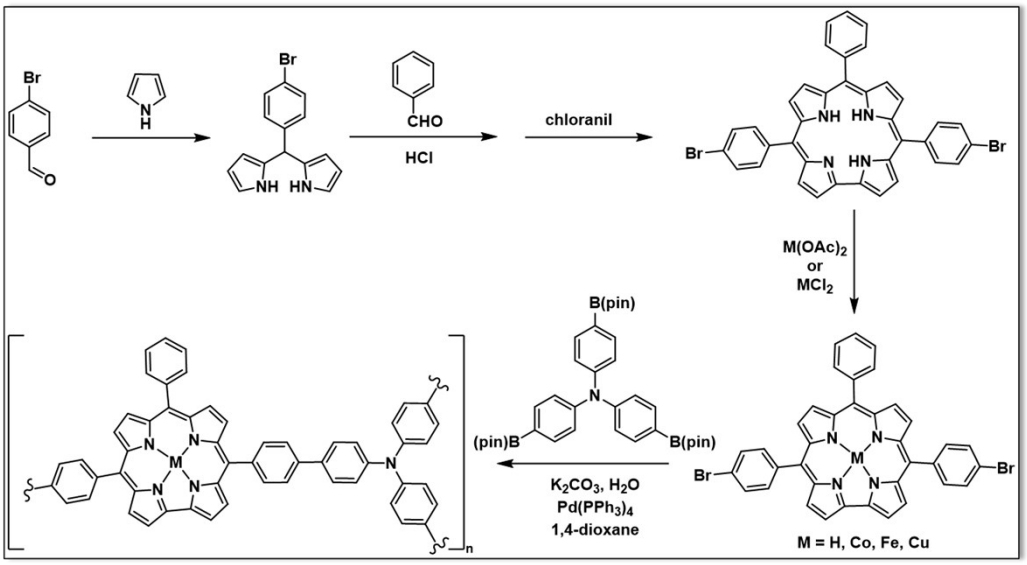

Scheme S1. Synthetic route of metal corroles.

Synthesis of 5-(4-bromophenyl)-dipyrromethane:

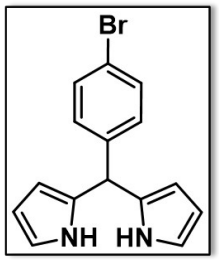

4-bromobenzaldehyde (2 g, 10.80 mmol), and freshly distilled pyrrole (50 ml, 723 mmol) were mixed under inert atmosphere. $InCl_3$ (0.24 g, 1.08 mmol) was added and the mixture was stirred for 2 h at room temperature. Then, powdered NaOH (0.4 g, 10 mmol) was added and the mixture was stirred for an additional 1 h. After filtration, the filtrate was concentrated under vacuum and the crude product was purified by silica-gel column chromatography (DCM: hexane = 1: 2) to afford the product as a yellow solid (2.84 g, 86%). ^{1}H NMR (500 MHz, Chloroform-d) δ 7.98 -

7.81 (br, 2H), 7.44 (d, J = 8.4 Hz, 2H), 7.09 (d, J = 8.5 Hz, 2H), 6.70 (d, J = 2.0 Hz, 2H), 6.17 (d, J = 2.8 Hz, 2H), 5.90 (s, 1H), 5.43 (s, 1H). ^{13}C NMR (126 MHz, Chloroform-d) δ 141.22, 131.73, 130.17, 120.88, 117.55, 108.61, 107.48, 43.45. HRMS (ESI) calcd for $C_{15}H_{13}BrN_2^+$ $(M+H)^+$: 301.0166, found: 299.0178.

Synthesis of 10-phenyl-5,15-(4-bromophenyl)-corrole

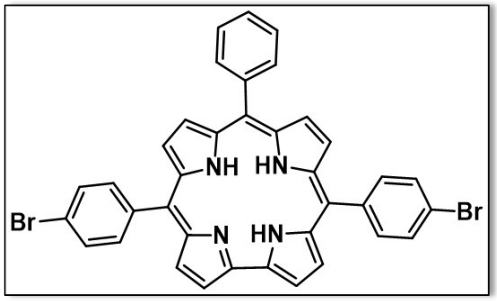

Benzaldehyde (200 mg, 1.88 mmol) and 5-(4-bromophenyl)-dipyrromethane (1.13 g, 3.75 mmol) were dissolved in a mixture of MeOH (100 mL), H_2O (100 mL), and HCl (6 mL, 36 %). The mixture was stirred for 2 h at room temperature. Then it was extracted with DCM, the organic phase was washed three times with water, dried over Na_2SO_4. After that, chloranil (1.39 g, 5.64 mmol) was added, and the resulted solution was stirred for another 2 h under dark. The solution was evaporated and then filtered through a pad of silica with DCM until the eluting solution was pale brown. The organic phase was concentrated, and then the crude product was purified by silica-gel chromatography (DCM: hexane = 1: 2) to afford the product as a purple solid (192 mg, 15%). ^{1}H NMR (400 MHz, Chloroform-d) δ 8.85 (d, J = 20.2 Hz, 4H), 8.47 (d, J = 70.4 Hz, 8H), 7.84 (d, J = 26.2 Hz, 7H), 7.47 (s, 2H). HRMS (ESI) calcd for $C_{37}H_{24}Br_2N_4^+$ $(M+H)^+$: 685.0423, found: 683.0440.

Synthesis of Co complex of 10-phenyl-5,15-(4-bromophenyl)-corrole

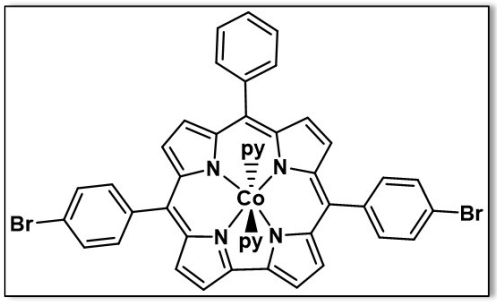

10-phenyl-5,15-(4-bromophenyl)-corrole (136 mg, 0.2 mmol) and $Co(OAc)_2$ $4H_2O$ (250 mg, 1.0 mmol) were dissolved in 10 mL pyridine. The solution was refluxed for 15 min, and the solvent was then evaporated using a rotavap. The crude product was purified by silica-gel chromatography (DCM: pyridine = 1: 0.01) to afford a purple solid. Subsequent recrystallization from

DCM/heptane afforded purple plates of Co corrole (122 mg, yield 80%). ^{1}H NMR (500 MHz, Chloroform-d) δ 8.86 (m, 4H), 8.22 - 7.45 (m, 13H), 6.28 (s, 4H), 5.66 (s, 4H), 3.14 (s, 2H), 1.08 (m, 4H). HRMS (ESI) calcd for $C_{37}H_{21}Br_2CoN_4^+$ $(M\text{-}2py)^+$: 739.9439, found: 739.9459.

Synthesis of Fe complex of 10-phenyl-5,15-(4-bromophenyl)-corrole

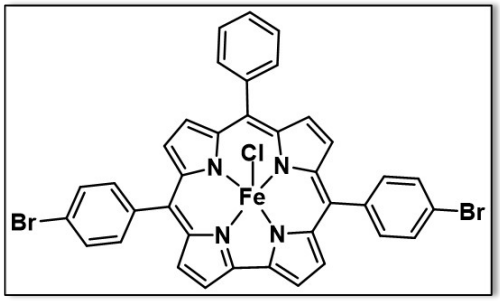

10-phenyl-5,15-(4-bromophenyl)-corrole (136 mg, 0.2 mmol) and $FeCl_2$ (127 mg, 1.0 mmol) were dissolved in 15 mL DMF. The solution was refluxed for 4 h under N_2, and the solvent was then evaporated using a rotavap. The crude product was purified by silica gel chromatography (DCM) to afford a purple solid. Subsequent recrystallization from DCM/heptane afforded purple plates of Fe corrole (109 mg, yield 70%). HRMS (ESI) calcd for $C_{38}H_{24}Br_2FeN_4^+$ $(M\text{-}Cl)^+$: 736.9468, found: 734.9477.

Synthesis of Cu complex of 10-phenyl-5,15-(4-bromophenyl)-corrole

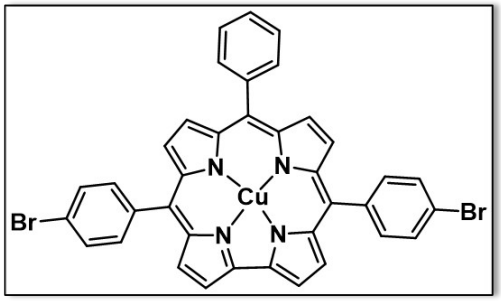

10-phenyl-5,15-(4-bromophenyl)-corrole (136 mg, 0.2 mmol) and $Cu(OAc)_2$ H_2O (200 mg, 1.0 mmol) were dissolved in a mixture of C_2H_5OH (50 mL) and DCM (10 mL). The mixture was stirred for 15 min at room temperature in the dark. Then it was extracted with DCM, the organic phase was washed three times with water, dried over Na_2SO_4. The organic phase was concentrated, and then the crude product was purified by silica-gel chromatography (DCM: hexane = 1: 2) to afford the product as a brown color solid (126 mg, 85%). HRMS (ESI) calcd for $C_{37}H_{21}Br_2CuN_4^+$ $(M+H)^+$: 743.9409, found: 741.9423.

Synthesis of tri[4-(4,4,5,5-tetramethyl-1,3,2-dioxaborolan-2-yl)phenyl]amine

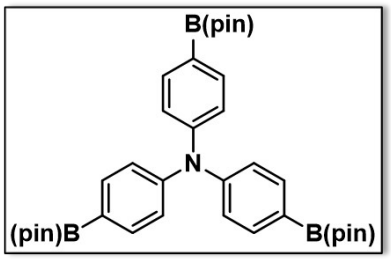

Tris(4-bromophenyl)amine (2 g, 4.15 mmol), bis(pinacolato)diboron (3.69 g, 14.5 mmol), CH_3CO_2K (1.22 g, 12.4 mmol), and $Pd(dppf)Cl_2$ (152 mg, 0.20 mmol) were dissolved in 50 ml 1,4-dioxane under inert atmosphere and then heated to 100 °C for 12 h. The resulting suspension was extracted with DCM and dried over $MgSO_4$. After the organic solvent was removed under vacuum, the crude product was purified by silica-gel chromatography (DCM: hexane = 1: 2) to afford the product as a white solid (2.59 g, 73%). ^{1}H NMR (500 MHz, Chloroform-d) δ 7.68 (d, J = 8.5 Hz, 6H), 7.08 (d, J = 8.5 Hz, 6H), 1.34 (s, 36H). HRMS (ESI) calcd for $C_{36}H_{48}B_3NO_6$ $(M+Na)^+$: 646.3673, found: 646.3653.

3. Analytical Data

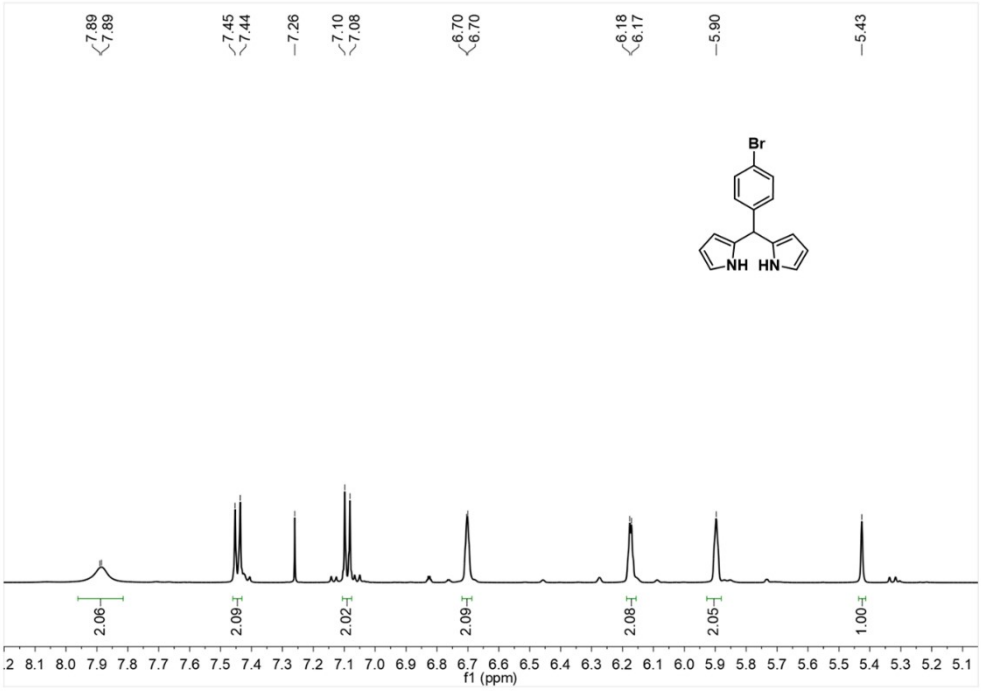

Fig. S1 ^{1}H NMR spectrum of 5-(4- bromophenyl)dipyrromethane in $CDCl_3$.

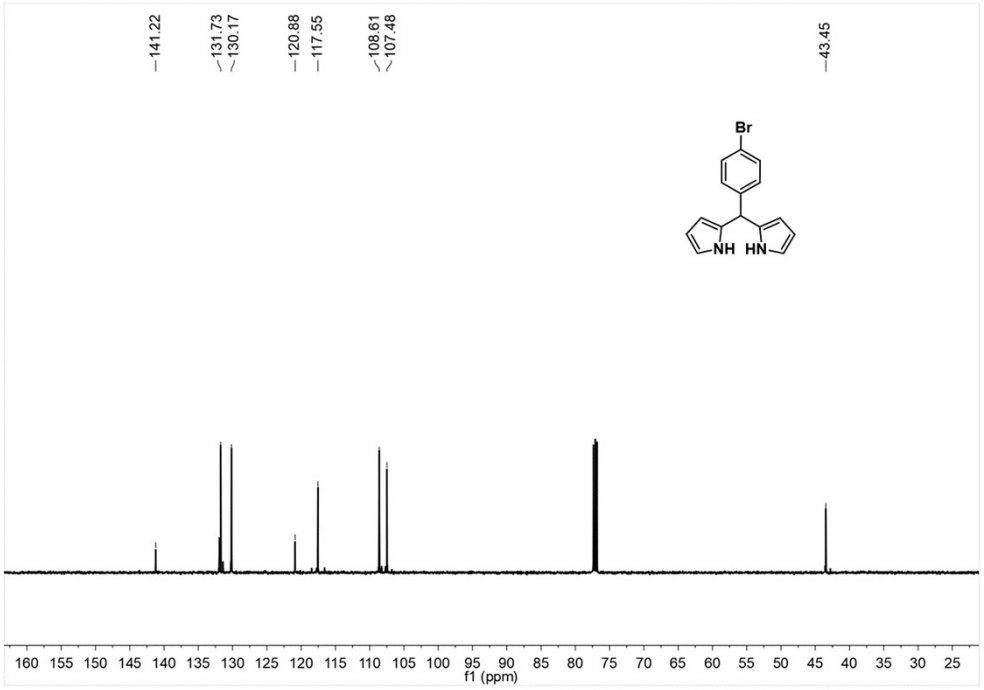

Fig. S2 ^{13}C NMR spectrum of 5-(4- bromophenyl)dipyrromethane in $CDCl_3$.

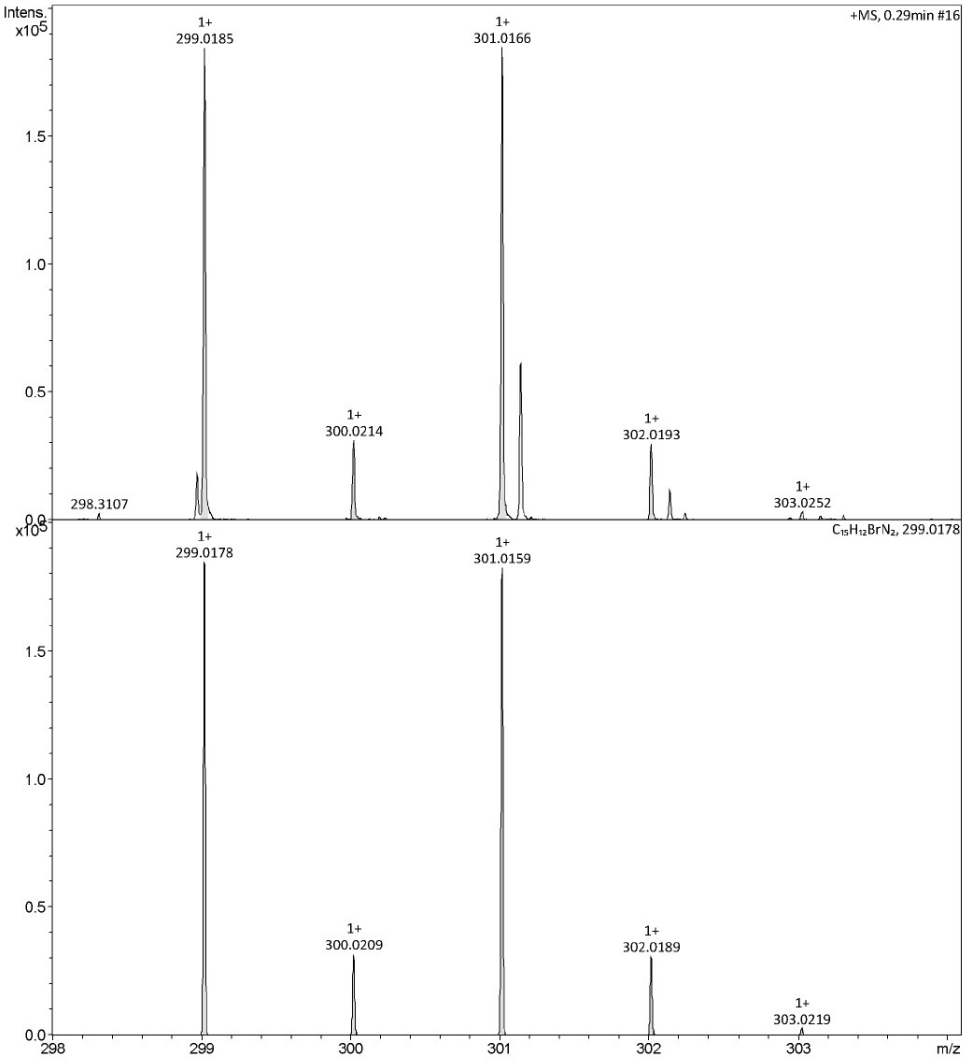

Fig. S3 HRMS spectrum of 5-(4- bromophenyl)dipyrromethane

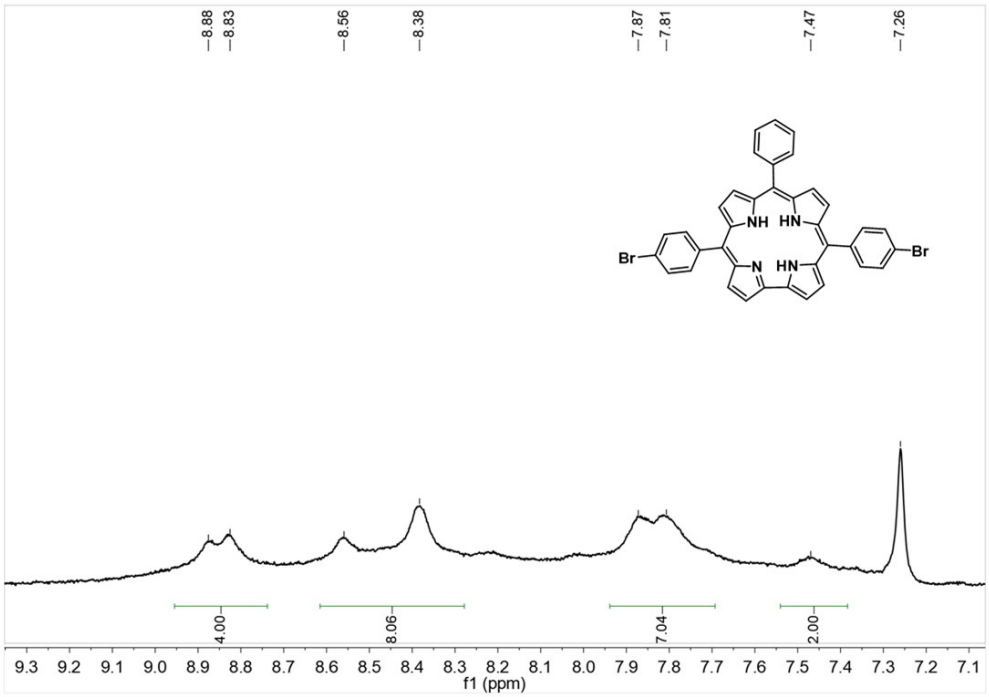

Fig. S4 ^{1}H NMR spectrum of 10-phenyl-5,15-(4-bromophenyl)-corrole in $CDCl_3$.

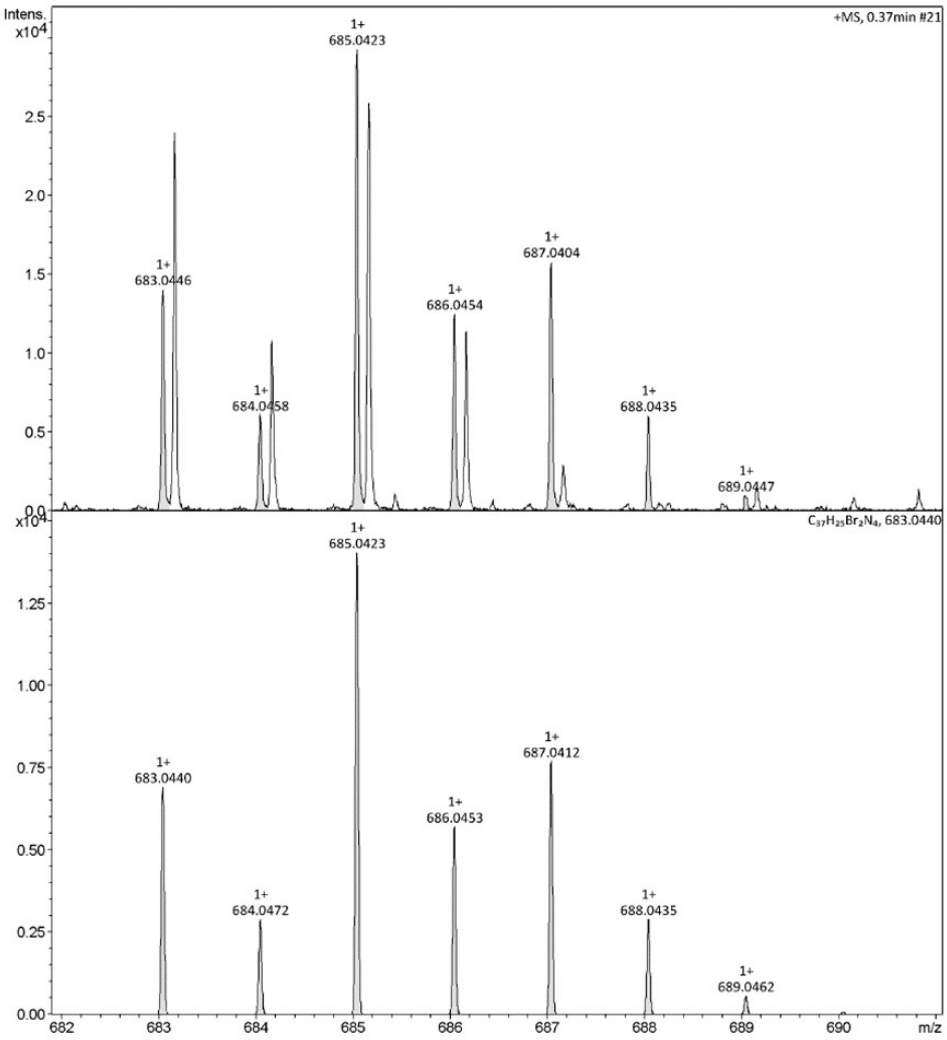

Fig. S5 HRMS spectrum of 10-phenyl-5,15-(4-bromophenyl)-corrole

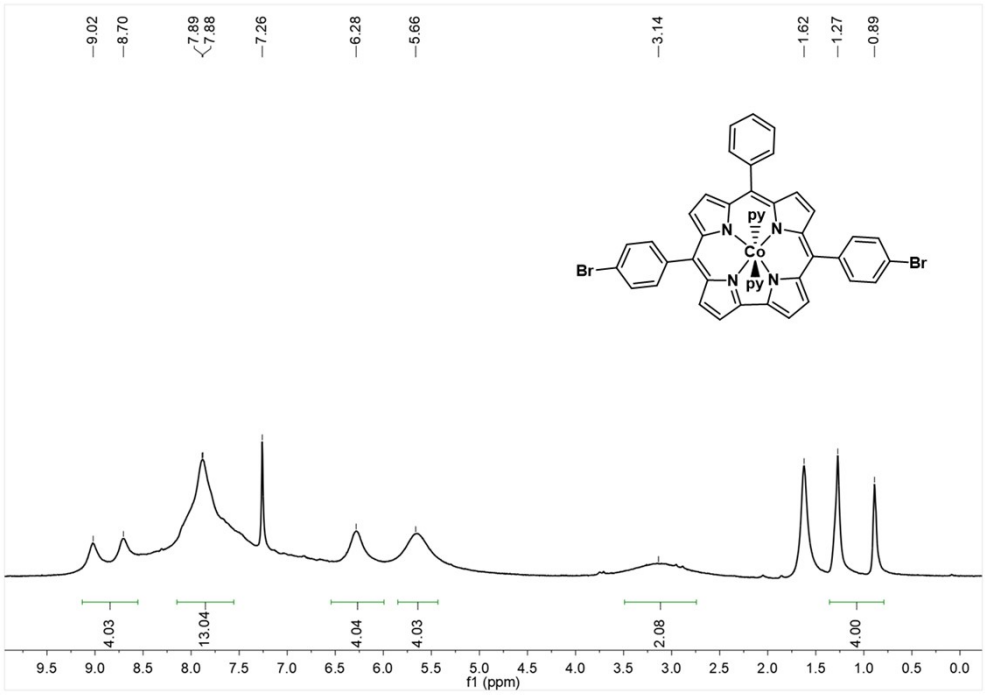

Fig. S6 ^{1}H NMR spectrum of Co complex of 10-phenyl-5,15-(4-bromophenyl)-corrole in $CDCl_3$.

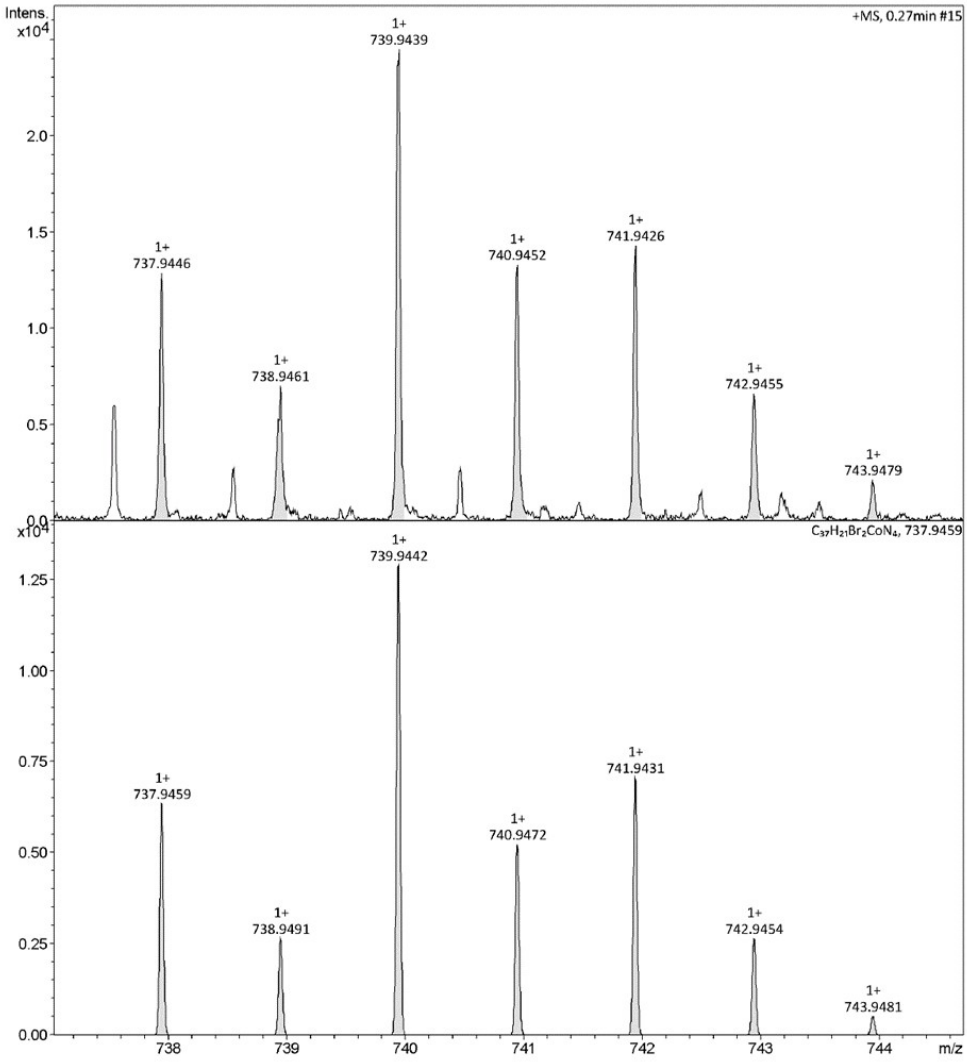

Fig. S7 HRMS spectrum of Co complex 10-phenyl-5,15-(4-bromophenyl)-corrole

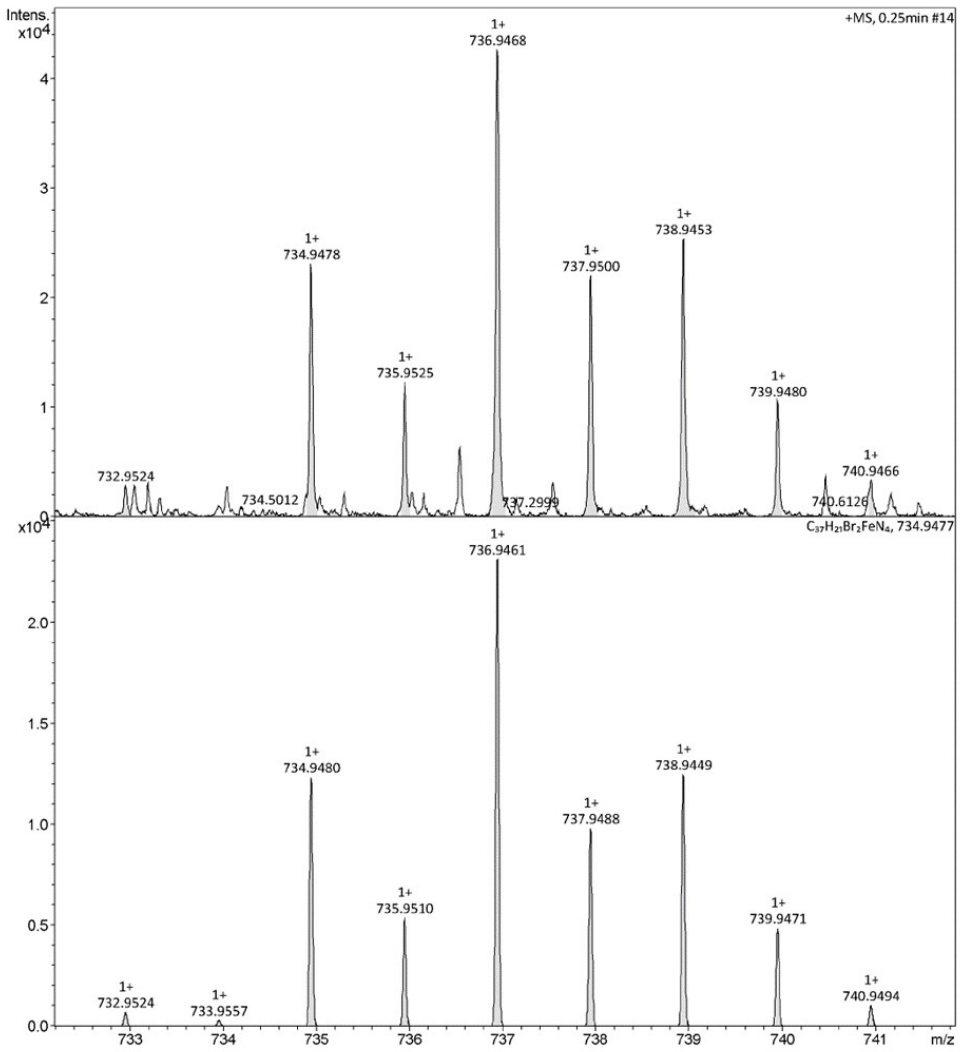

Fig. S8 HRMS spectrum of Fe complex 10-phenyl-5,15-(4-bromophenyl)-corrole

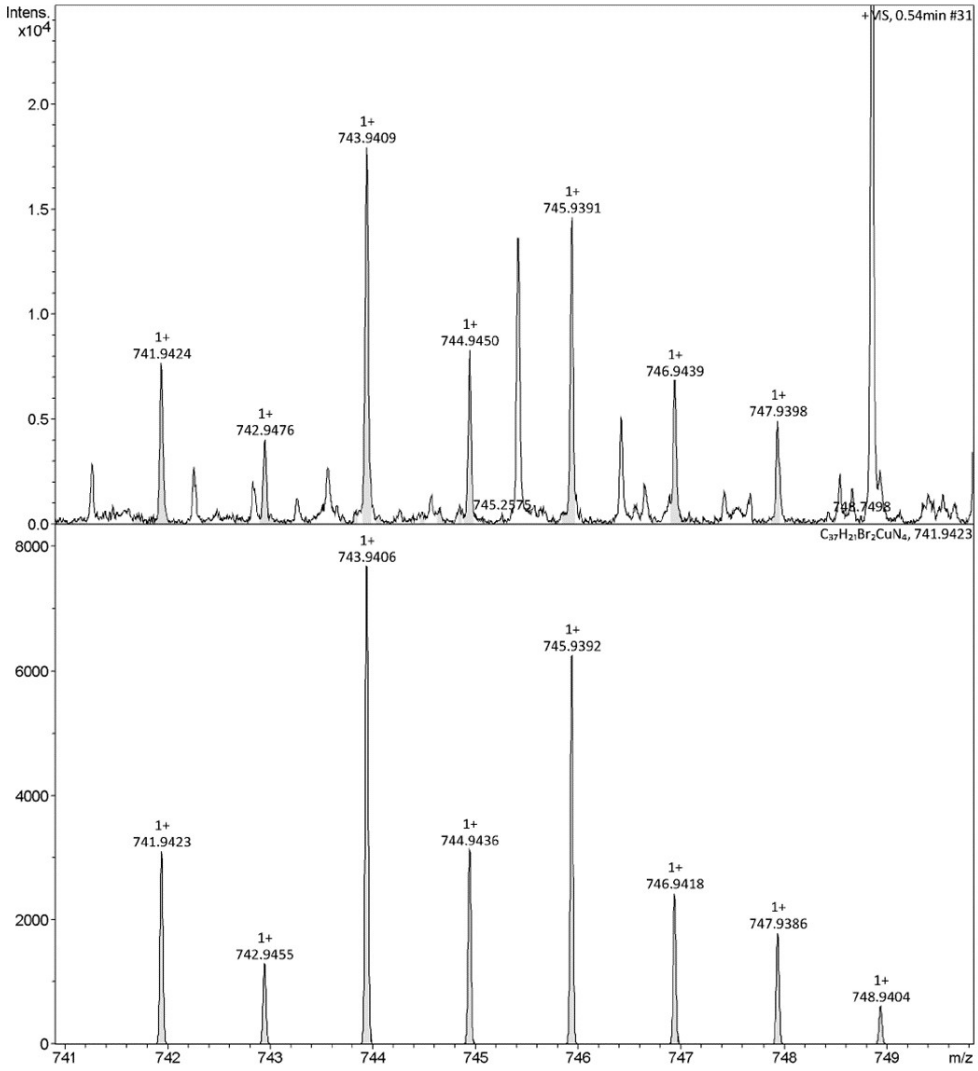

Fig. S9 HRMS spectrum of Cu complex 10-phenyl-5,15-(4-bromophenyl)-corrole

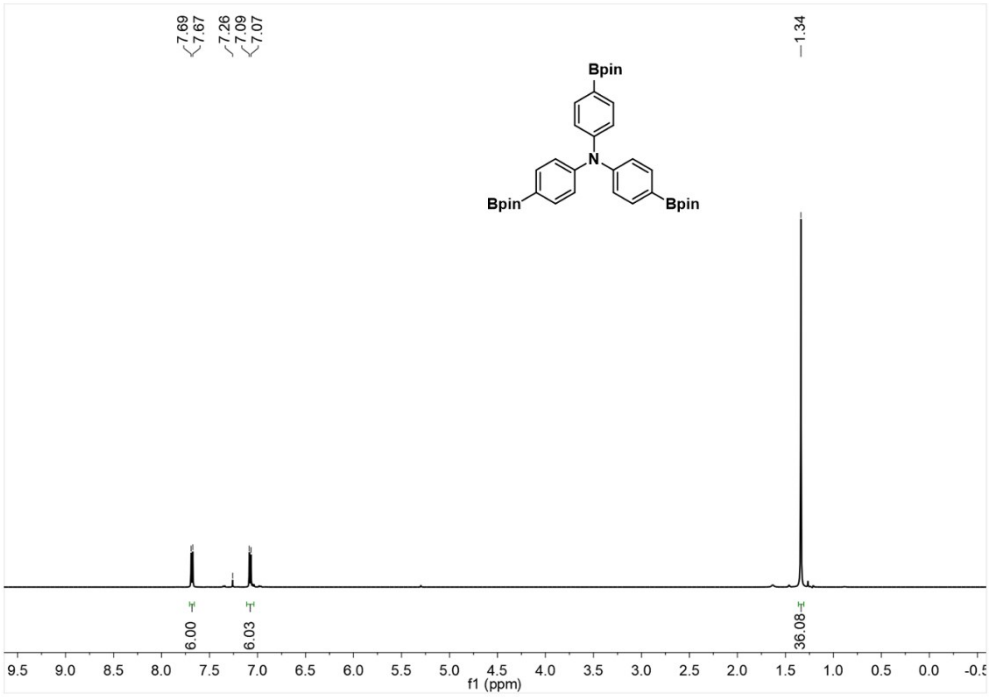

Fig. S10 ^{1}H NMR spectrum of tri[4-(4,4,5,5-tetramethyl-1,3,2-dioxaborolan-2-yl)phenyl]amine in $CDCl_3$.

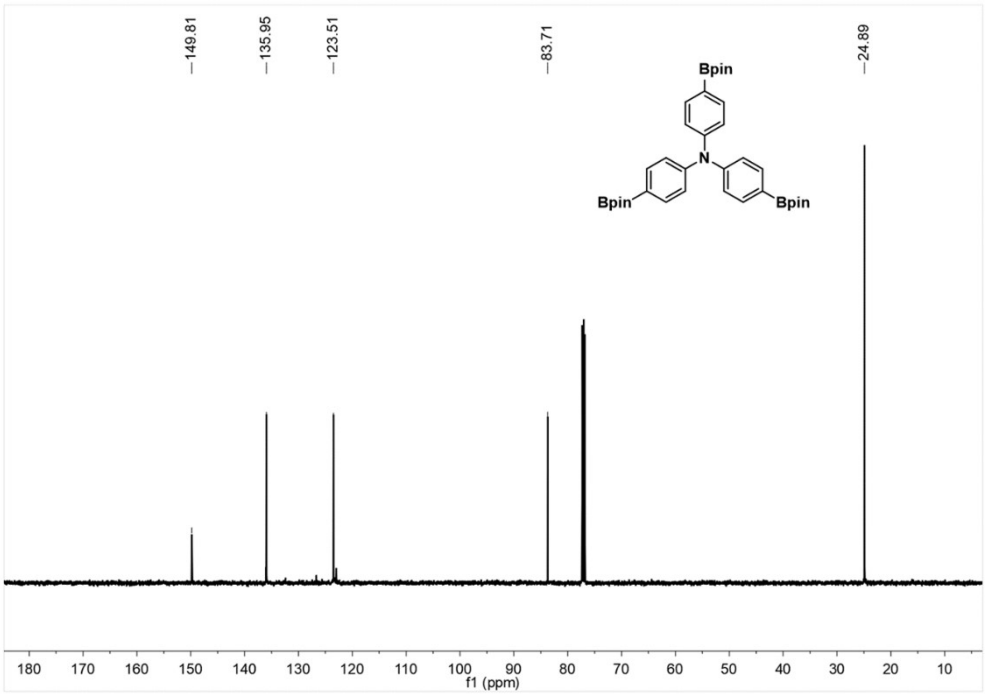

Fig. S11 ^{13}C NMR spectrum of tri[4-(4,4,5,5-tetramethyl-1,3,2-dioxaborolan-2-yl)phenyl]amine in $CDCl_3$.

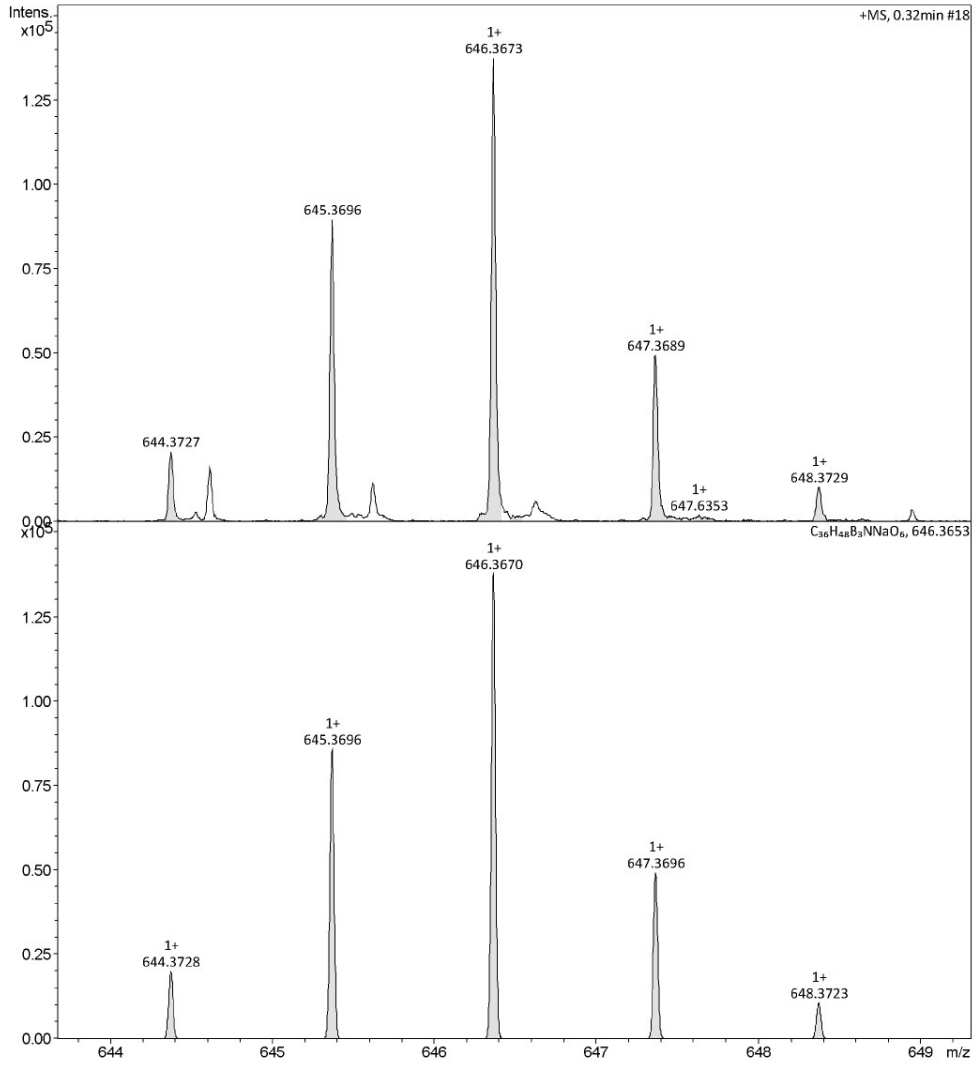

Fig. S12 HRMS spectrum of tri[4-(4,4,5,5-tetramethyl-1,3,2-dioxaborolan-2-yl)phenyl]amine

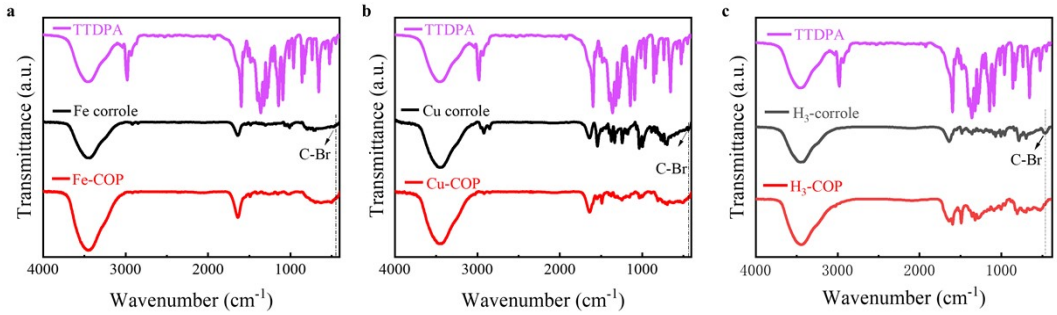

Fig. S13 Infrared spectra of (a) Fe-COP, (b) Cu-COP, and (c) H_3-COP.

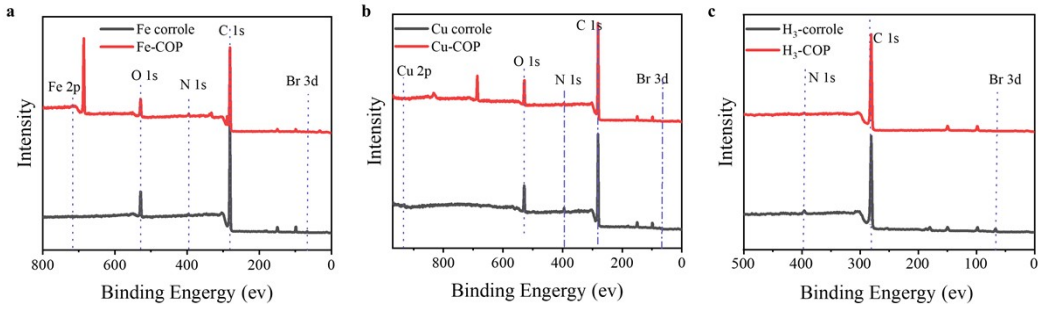

Fig. S14 XPS survey scan spectra of (a) Fe-COP and Fe corrole, (b) Cu-COP and Cu corrole, (c) H_3-COP. and H_3 corrole

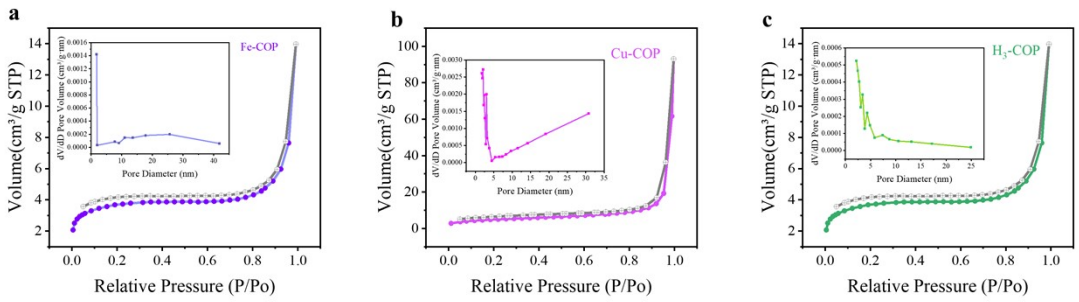

Fig. S15 XPS survey scan spectra of (a) Fe-COP and Fe corrole, (b) Cu-COP and Cu corrole, (c) H_3-COP. and H_3 corrole

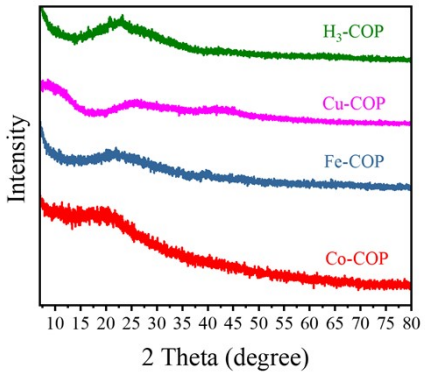

Fig. S16 XRD patterns of Co-COP, Fe-COP, Cu-COP, H_3-COP, respectively.

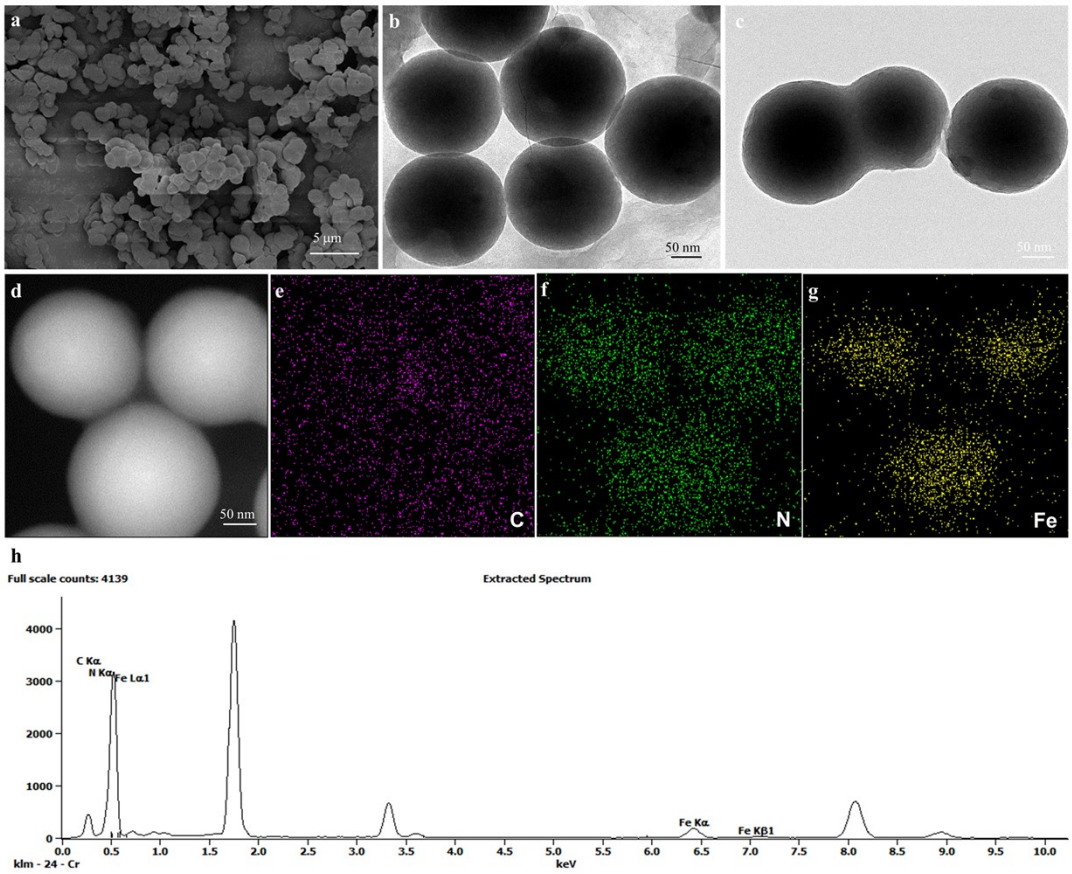

Fig. S17 Morphological and compositional characterizations of Fe-COP. a) SEM image. b, c) TEM images. d) HAADF-STEM image and e-g) Corresponding elemental mapping images of Fe-COP. h) EDX spectrum.

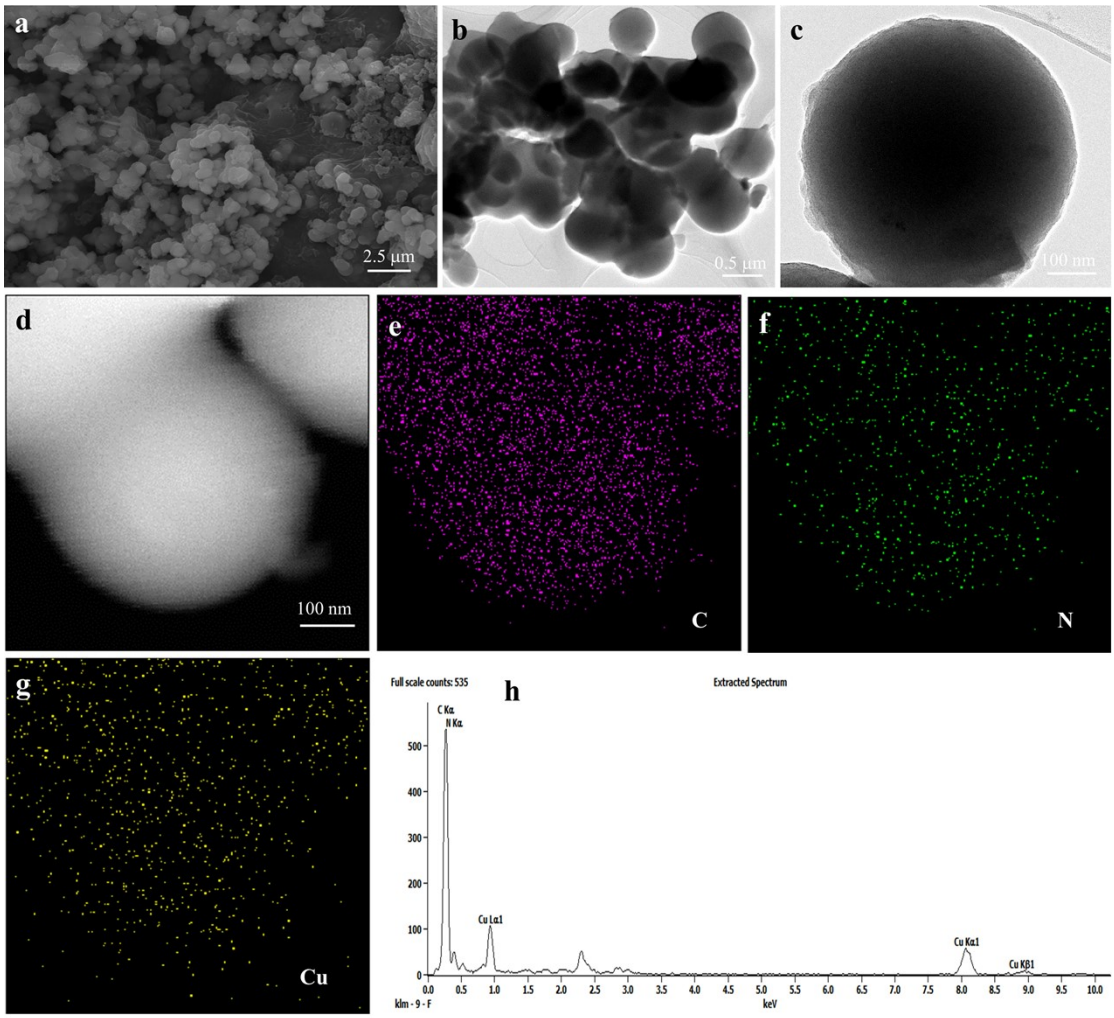

Fig. S18 Morphological and compositional characterizations of Cu-COP. a) SEM image. b, c) TEM images. d) HAADF-STEM image and e-g) Corresponding elemental mapping images of Cu-COP. h) EDX spectrum.

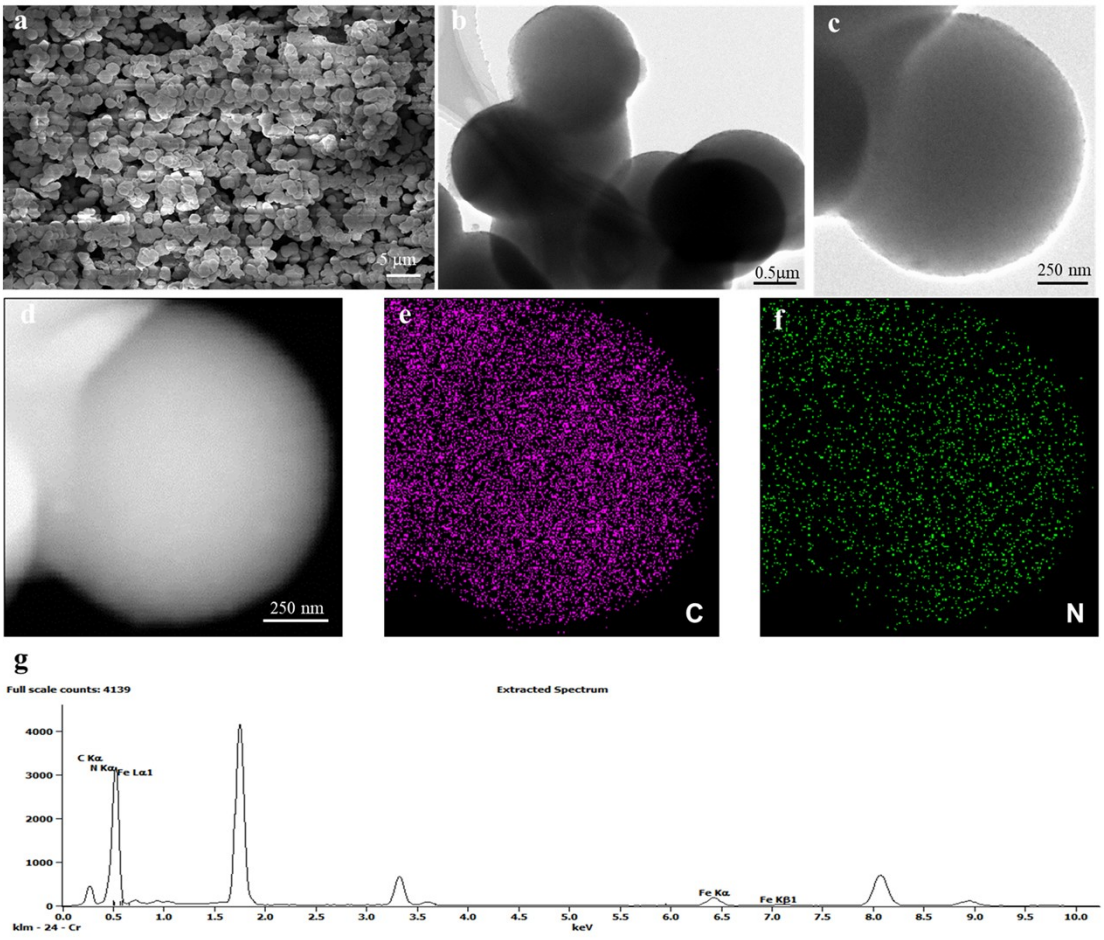

Fig. S19 Morphological and compositional characterizations of H_3-COP. a) SEM image. b, c) TEM images. d) HAADF-STEM image and e, f) Corresponding elemental mapping images of H_3-COP. g) EDX spectrum.

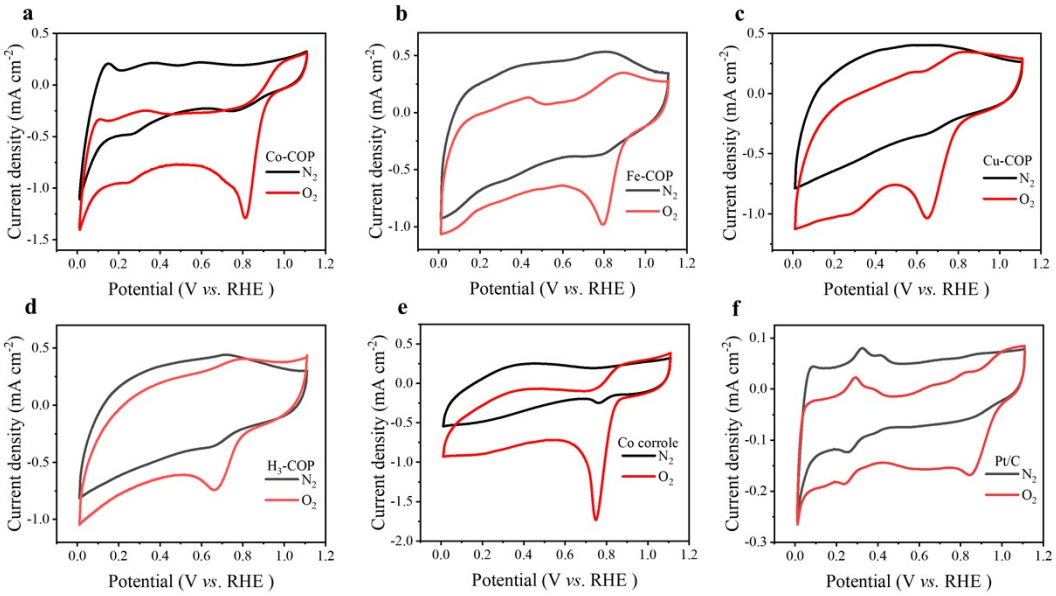

Fig. S20 CV curves in N_2/O_2-saturated 0.1 M KOH solution at 50 mv s^{-1}; a) CV curves of Co-COP. b) CV curves of Fe-COP. c) CV curves of Cu-COP. d) CV curves of H_3-COP. e) CV curves of Co corrole. f) CV curves of Pt/C.

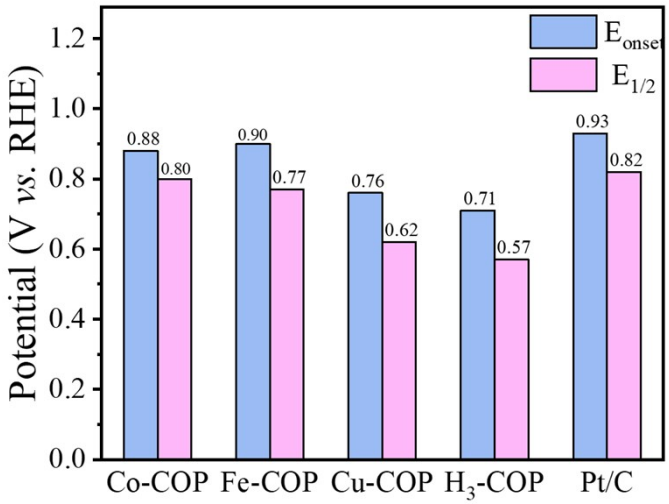

Fig. S21 Initial potential and half-wave potential of Co-COP, Fe-COP, Cu-COP, H_3-COP and Pt/C.

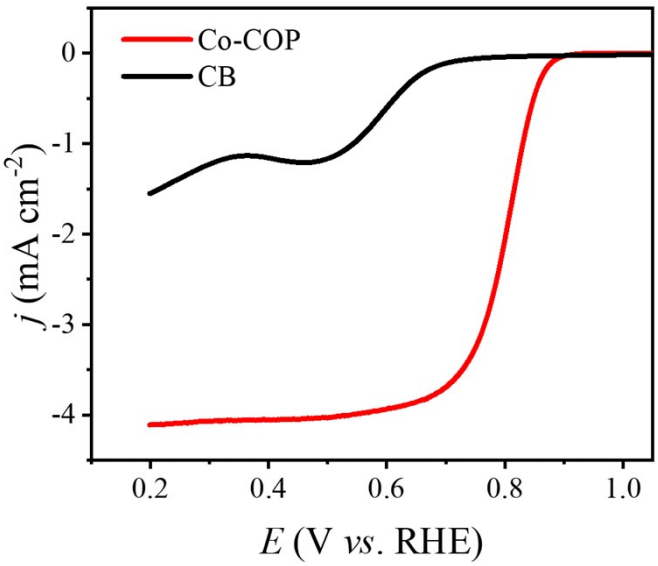

Fig. S22 a) ORR LSVs of Co-COP and unmodified CB at a scan rate of 5 mV s^{-1} and 1600 rpm in O_2-saturated 0.1 M KOH solution.

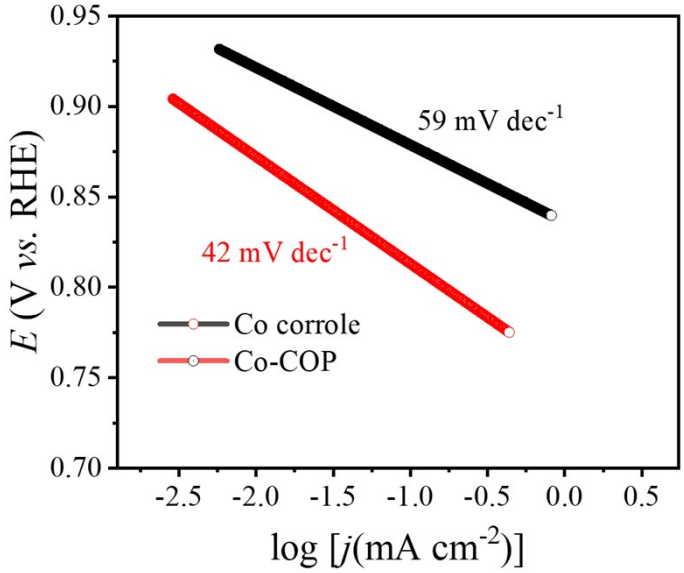

Fig. S23 ORR Tafel slopes derived from the corresponding polarization curves of Co-COP and Co corrole.

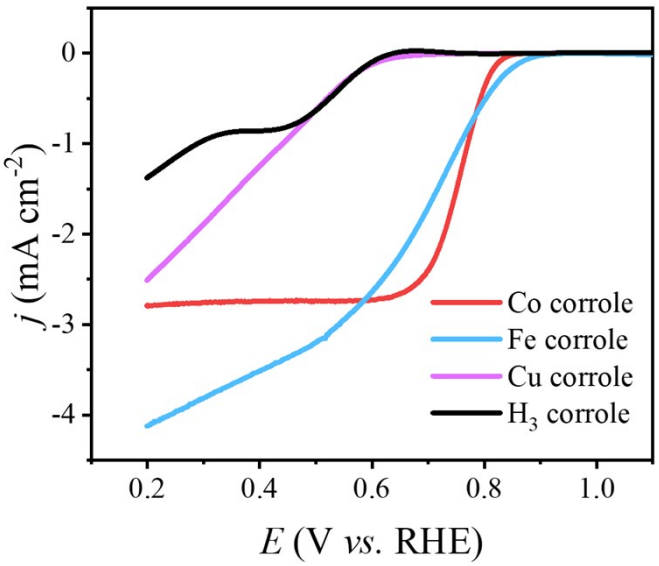

Fig. S24 ORR LSVs of Co corrole, Fe corrole, Cu corrole, and H_3 corrole at 1600 rpm rotation rate in 0.1 M KOH solutions.

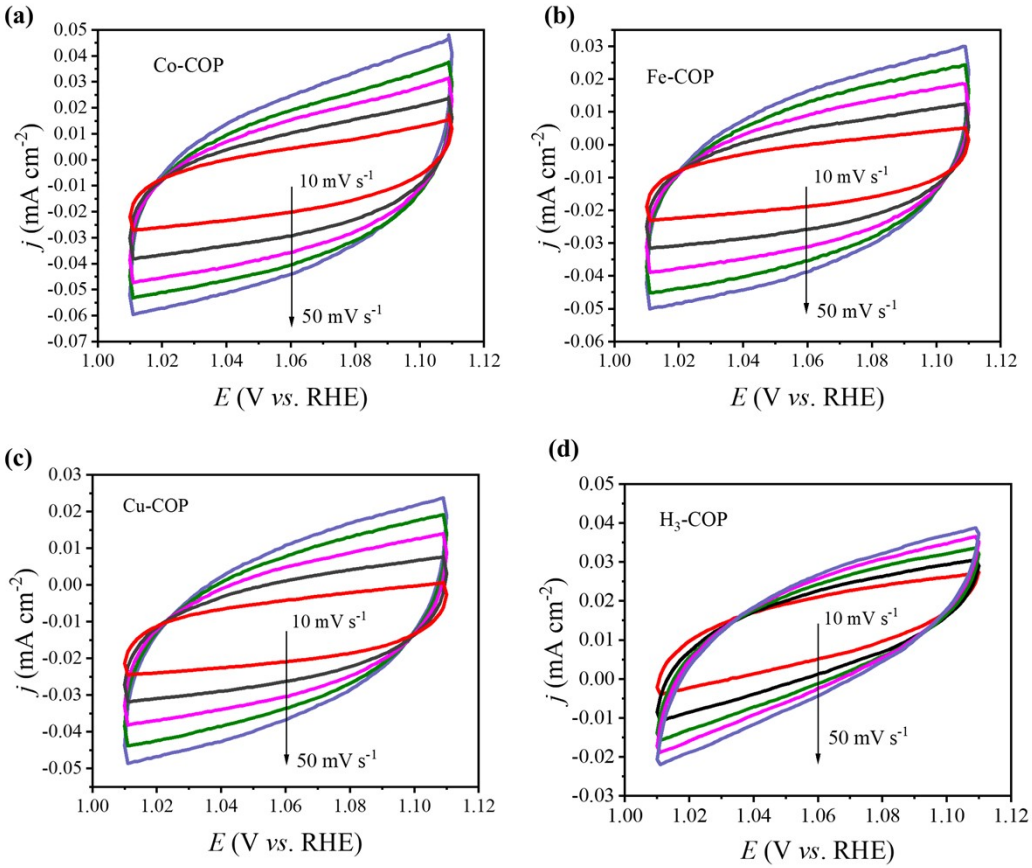

Fig. S25 ORR CV measurements at different scan rates for (a) Co-COP, (b) Fe-COP, (c) Cu-COP, and (d) H_3-COP.

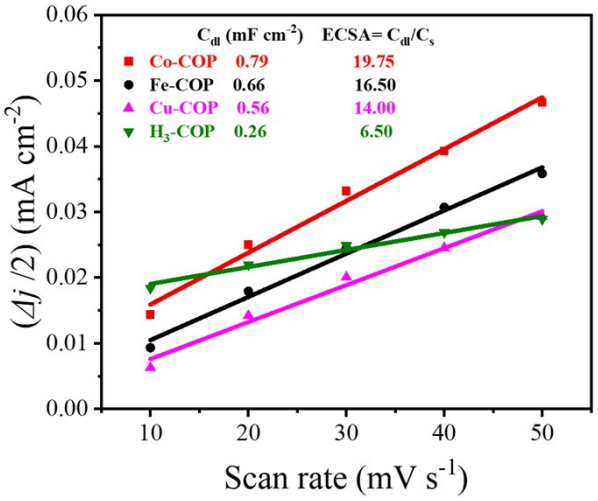

Fig. S26 ECSA values estimated from double-layer capacitance (*C*dl) data.

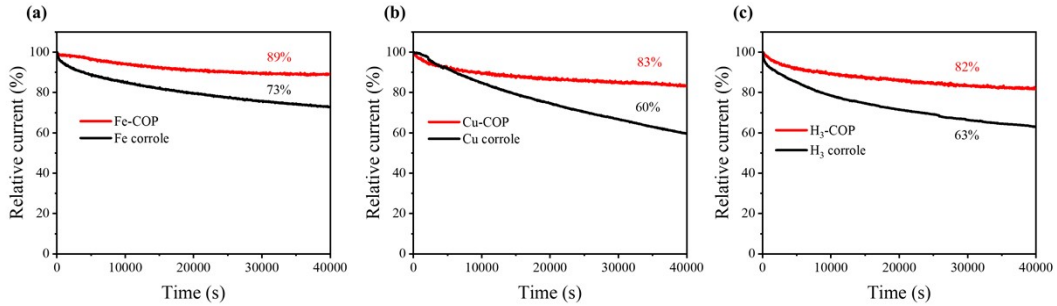

Fig. S27 The stability assessment of (a) Fe-COP, Fe corrole, (b) Cu-COP, Cu corrole and (c) H_3-COP, H_3 corrole.

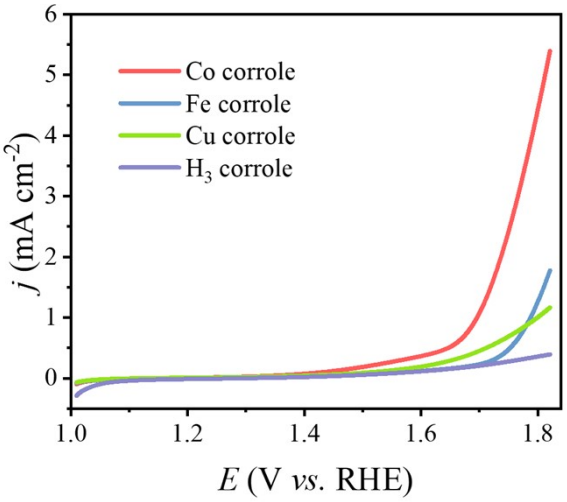

Fig. S28 OER LSVs of Co corrole, Fe corrole, Cu corrole, and H_3 corrole at 1600 rpm rotation rate in 0.1 M KOH solutions.

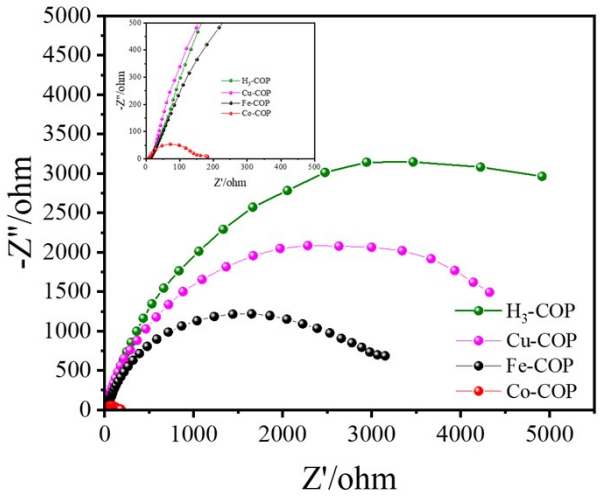

Fig. S29 HER EIS spectra for Co-COP, Fe-COP, Cu-COP, and H_3-COP.

Table. S1 Literature comparison of ORR performances with other COPs based catalysts.

Catalyst	Electrolyte	Half-wave potential (V vs. RHE)	Onset potential (V vs. RHE)	Reference
Co-COP	0.1M KOH	0.80	0.88	This work
TPA-tpd-Co	0.1M KOH	-	0.80	[1]
CoTAPP-NA	0.1M KOH	0.84	0.95	[2]
PPy/FeTCPP/Co	0.1M KOH	0.86	1.01	[3]
COP-PSO_3-Co-rGO	0.1M KOH	0.72	0.88	[4]
NDI-COF/GC	0.1 M NaOH	0.63	0.75	[5]
CoCOF-PyrGO	0.1 M KOH	0.74	0.82	[6]
Co-POP	0.1 M KOH	0.87	-	[7]
Co@TBPA-phen	1.0 M KOH	-	0.82	[8]
FeNi-COP-800	1.0 M KOH	0.80	-	[9]
Co porphyrin@ZIF-67	0.1 M KOH	0.79	-	[10]
PCN-226-Co/C	0.1 M KOH	0.75	0.83	[11]

Table. S2 Literature comparison of OER performances with other COPs based catalysts.

Catalyst	Electrolyte	Overpotential (mV, at 10 mA·cm^{-2})	Tafel Slope (mV dec^{-1})	Reference
Co-COP	0.1M KOH	560	96	This work
TPA-tpd-Co	0.1M KOH	440	42	[1]
CoTAPP-NA	1.0 M KOH	416	68	[2]
Ni-TAPP- NA	1.0 M KOH	486	81	[2]
PPy/FeTCPP/Co	1.0 M KOH	380	61	[3]
Cu-CMP900	1.0 M KOH	560	80	[12]
CoCOP	1.0 M KOH	350	151	[13]
Co-POP	1.0 M KOH	340	93	[7]
zCo@TBPA-phen	1.0 M KOH	480	115	[8]
FeNi-COP-800	1.0 M KOH	400	103	[9]
PCN-226-Co/C	1.0 M KOH	440	111	[11]
Pb-TCPP	1.0 M KOH	470	106	[14]
CoP-2ph-CMP-800	1.0 M KOH	370	86	[15]

Table. S3 Literature comparison of HER performances with other COPs based catalysts.

Catalyst	Electrolyte	Overpotential (mV, at 10 mA·cm^{-2})	Tafel Slope (mV dec^{-1})	Reference
Co-COP	0.1M KOH	208	83	This work
TPA-tpd-Co	0.1M KOH	428	-	[1]
CoTAPP-NA	1.0 M KOH	470	110	[2]
PPy/FeTCPP/Co	1.0 M KOH	240	83	[3]
Cu-CMP900	1.0 M KOH	430	135	[12]
CoCOP	1.0 M KOH	310	161	[13]
Co@TBPA-phen	0.5 M H_2SO_4	335	115	[8]
CoP-2ph-CMP-800	1.0 M KOH	360	121	[15]
CoTCPP polymer	0.5 M H_2SO_4	475	197	[16]
COF-Ni$(OH)_2$	1.0 M KOH	258	38.9	[17]
TiCP-PCP	0.5 M H_2SO_4	339	142	[18]

References:

[1] S. Singh, M.K. Ghorai, K.K. Kar, Cobalt(ii)-bridged triphenylamine and terpyridine-based donor-acceptor coordination polymer as an efficient trifunctional electrocatalyst, J Mater Chem a 11 (2023) 8003-8012.

[2] G. Cai, L. Zeng, L. He, S. Sun, Y. Tong, J. Zhang, Imine Gels Based on Ferrocene and Porphyrin and Their Electrocatalytic Property, Chemistry-An Asian Journal 15 (2020) 1963-1969.

[3] J. Yang, X. Wang, B. Li, L. Ma, L. Shi, Y. Xiong, H. Xu, Novel Iron/Cobalt-Containing Polypyrrole Hydrogel-Derived Trifunctional Electrocatalyst for Self-Powered Overall Water Splitting, Adv Funct Mater 27 (2017) 1606497.

[4] J. Guo, C. Lin, Z. Xia, Z. Xiang, A Pyrolysis-Free Covalent Organic Polymer for Oxygen Reduction, Angewandte Chemie International Edition 57 (2018) 12567-12572.

[5] S. Royuela, E. Martínez-Periñán, M.P. Arrieta, J.I. Martínez, M.M. Ramos, F. Zamora, E. Lorenzo, J.L. Segura, Oxygen reduction using a metal-free naphthalene diimide-based covalent organic framework electrocatalyst, Chem Commun 56 (2020) 1267-1270.

[6] Q. Zuo, G. Cheng, W. Luo, A reduced graphene oxide/covalent cobalt porphyrin framework for efficient oxygen reduction reaction, Dalton T 46 (2017) 9344-9348.

[7] H. Lei, Q. Zhang, Z. Liang, H. Guo, Y. Wang, H. Lv, X. Li, W. Zhang, U. Apfel, R. Cao, Metal-Corrole-Based Porous Organic Polymers for Electrocatalytic Oxygen Reduction and

Evolution Reactions, Angewandte Chemie International Edition 61 (2022) e202201104.
[8] S. Singh, M.K. Ghorai, K.K. Kar, A cobalt harnessed phenanthroline and triphenylamine-based conjugated mesoporous polymer designed by a donor-acceptor approach for trifunctional electrocatalysis, J Mater Chem a (2023).
[9] Z. Liao, Y. Wang, Q. Wang, Y. Cheng, Z. Xiang, Bimetal-phthalocyanine based covalent organic polymers for highly efficient oxygen electrode, Applied Catalysis B: Environmental 243 (2019) 204-211.
[10] Z. Liang, H. Guo, G. Zhou, K. Guo, B. Wang, H. Lei, W. Zhang, H. Zheng, U. Apfel, R. Cao, Metal-Organic-Framework-Supported Molecular Electrocatalysis for the Oxygen Reduction Reaction, Angewandte Chemie International Edition 60 (2021) 8472-8476.
[11] M.O. Cichocka, Z. Liang, D. Feng, S. Back, S. Siahrostami, X. Wang, L. Samperisi, Y. Sun, H. Xu, N. Hedin, H. Zheng, X. Zou, H. Zhou, Z. Huang, A Porphyrinic Zirconium Metal–Organic Framework for Oxygen Reduction Reaction: Tailoring the Spacing between Active-Sites through Chain-Based Inorganic Building Units, J Am Chem Soc 142 (2020) 15386-15395.
[12] S. Cui, M. Qian, X. Liu, Z. Sun, P. Du, A Copper Porphyrin-Based Conjugated Mesoporous Polymer-Derived Bifunctional Electrocatalyst for Hydrogen and Oxygen Evolution, Chemsuschem 9 (2016) 2365-2373.
[13] A. Wang, L. Cheng, W. Zhao, X. Shen, W. Zhu, Electrochemical hydrogen and oxygen evolution reactions from a cobalt-porphyrin-based covalent organic polymer, J Colloid Interf Sci 579 (2020) 598-606.
[14] F. Dai, W. Fan, J. Bi, P. Jiang, D. Liu, X. Zhang, H. Lin, C. Gong, R. Wang, L. Zhang, D. Sun, A lead-porphyrin metal-organic framework: gas adsorption properties and electrocatalytic activity for water oxidation, Dalton T 45 (2016) 61-65.
[15] H. Jia, Y. Yao, Y. Gao, D. Lu, P. Du, Pyrolyzed cobalt porphyrin-based conjugated mesoporous polymers as bifunctional catalysts for hydrogen production and oxygen evolution in water, Chem Commun 52 (2016) 13483-13486.
[16] Y. Wu, J.M. Veleta, D. Tang, A.D. Price, C.E. Botez, D. Villagrán, Efficient electrocatalytic hydrogen gas evolution by a cobalt-porphyrin-based crystalline polymer, Dalton T 47 (2018) 8801-8806.
[17] D. Mullangi, V. Dhavale, S. Shalini, S. Nandi, S. Collins, T. Woo, S. Kurungot, R. Vaidhyanathan, Low-Overpotential Electrocatalytic Water Splitting with Noble-Metal-Free Nanoparticles Supported in a sp3 N-Rich Flexible COF, Adv Energy Mater 6 (2016) 1600110.
[18] A. Wang, L. Cheng, X. Shen, W. Zhu, L. Li, Mechanistic insight on porphyrin based porous titanium coordination polymer as efficient bifunctional electrocatalyst for hydrogen and oxygen evolution reactions, Dyes Pigments 181 (2020) 108568.